Electronic Supplementary Information

Photophysical Properties of trans-Platinum Acetylide Complexes Featuring NHC-Ligands

Russell W. Winkel, Galyna G. Dubinina, Khalil A. Abboud and Kirk S. Schanze*

Department of Chemistry, University of Florida, P.O.Box 117200, Gainesville, FL 32611

kschanze@chem.ufl.edu

[†] University of Florida

*Author to whom correspondence should be addressed. TEL: 352-392-9133, FAX: 352-392-2395, e-mail: kschanze@chem.ufl.edu

Contents: Pg. #

1. X-ray Experimental and Data

The asymmetric unit of **1** consists of a half Pt complex (located on an inversion center) and one chloroform solvent molecule in general position. The coordinated Cl ligand and one of the solvent Cl atoms are disordered and each was refined in two parts. In the solvent, the disorder in one Cl atom is accompanied with a smaller disorder in the chloroform C atom but this was not significant enough to be resolved. In the final cycle of refinement, 4584 reflections (of which 4224 are observed with $I > 2\sigma(I)$) were used to refine 225 parameters and the resulting R_1, wR_2 and S (goodness of fit) were 1.42%, 4.02% and 1.044, respectively.

The asymmetric unit of **2a** consists of a half Pt complex and a dichloromethane solvent molecule. In the final cycle of refinement, 5134 reflections (of which 4881 are observed with $I > 2\sigma(I)$) were used to refine 331 parameters and the resulting R_1, wR_2 and S (goodness of fit) were 2.50%, 6.29% and 1.085, respectively.

The asymmetric unit of **2b** consists of a half Pt complex and a dichloromethane solvent molecule (located on an inversion center). The C9 cyclohexyl group is disordered and refined in two parts. The methyl group at C31 is also disordered and refined in two parts. Each disordered region's parts were refined with their site occupation factors dependently refined. In the final cycle of refinement, 8708 reflections (of which 6184 are observed with $I > 2\sigma(I)$) were used to refine 422 parameters and the resulting R_1, wR_2 and S (goodness of fit) were 4.20%, 10.37% and 1.036, respectively.

The asymmetric unit of **2c** consists of a half Pt complex (located on an inversion center) and a dichloromethane solvent molecule. The ethyl group on C21 is disordered and was refined in two parts. In the final cycle of refinement, 9171 reflections (of which 9118 are observed with I

> $2\sigma(I)$) were used to refine 474 parameters and the resulting R_1, wR_2 and S (goodness of fit) were 2.53%, 6.33% and 1.040, respectively.

All refinements were carried out by minimizing the wR_2 function using F^2 rather than F values. R_1 is calculated to provide a reference to the conventional R value but its function is not minimized.

Table 1. Summary of Crystallographic Data[a]

	1·$CHCl_3$	**2a**·CH_2Cl_2	**2b**·CH_2Cl_2	**2c**·CH_2Cl_2
empirical formula	C32H50Cl8N4Pt	C63H68Cl2N4Pt	C84H92Cl4N6PtS2	C94H104Cl4N6Pt
fw	969.45	1232.13	1586.65	1654.72
λ [Å]	0.71073	1.54178	0.71073	0.71073
cryst syst	Monoclinic	Monoclinic	Monoclinic	Triclinic
space group	$P2_1/c$	$P2_1/c$	$P2_1/c$	$P1$
unit cell dimen				
a [Å]	10.7953(19)	9.0339(4)	8.2552(7)	9.9529(2)
b [Å]	14.724(3)	20.7765(9)	27.997(2)	13.1998(2)
c [Å]	12.701(2)	15.4670(6)	16.4264(14)	15.8601(3)
α [deg]	90	90	90	105.207(1)
β [deg]	97.930	101.326(2)	92.455(2)	93.171(1)
γ [deg]	90	90	90	93.064(1)
V [Å^3]	1999.6(6)	2846.5(2)	3793.1(6)	2002.60(6)
Z	2	2	2	1
ρ_{calcd} [Mg m^{-3}]	1.610	1.438	1.389	1.372
μ [mm^{-1}]	4.071	6.664	2.094	1.936
F(000)	968	1256	1632	856
crystal size, mm	0.21 x 0.20 x 0.19	0.25 x 0.15 x 0.07	0.24 x 0.10 x 0.07	0.18 x 0.14 x 0.08
θ range [deg]	1.90 to 27.50	5.16 to 68.00	1.45 to 27.50	1.79 to 27.50
index ranges (h,k,l)	-13,14; -15,19; -16,16	-10,10; -24,24; -18,18	-10,8; -35,36; -21,21	-12,12; -17,17; -20,20
no. reflns collected	23816	72981	34768	35226
no. indep reflns	4584 [R(int) = 0.0248]	5134 [R(int) = 0.0291]	8708 [R(int) = 0.0320]	9171 [R(int) = 0.0292]
no. relfns [$I>2\sigma(I)$]	4224	4881	6184	9118
max. and min. transmn	0.5118 and 0.4862	0.6454 and 0.2888	0.8724 and 0.6378	0.8605 and 0.7219
no. data/restraints/params	4584/0/225	5134/0/331	8708/36/422	9171/0/474
goodness-of-fit on F^2	1.044	1.085	1.036	1.040
final R indices [$I>2\sigma(I)$]	$R_1 = 0.0142$, $wR_2 = 0.0402$	$R_1 = 0.0250$, $wR_2 = 0.0629$	$R_1 = 0.0420$, $wR_2 = 0.1037$	$R_1 = 0.0253$, $wR_2 = 0.0633$
R indices (all data)	$R_1 = 0.0158$, $wR_2 = 0.0416$	$R_1 = 0.0261$, $wR_2 = 0.0643$	$R_1 = 0.0673$, $wR_2 = 0.1111$	$R_1 = 0.0256$, $wR_2 = 0.0636$
largest diff peak/hole [e Å^{-3}]	0.764 and -1.192	1.083 and -0.928	1.607 and -0.764	1.151 and -1.116

[a] Data common to all structures: temp of collection, 100(2) K; refinement method: full-matrix least-squares on F^2.

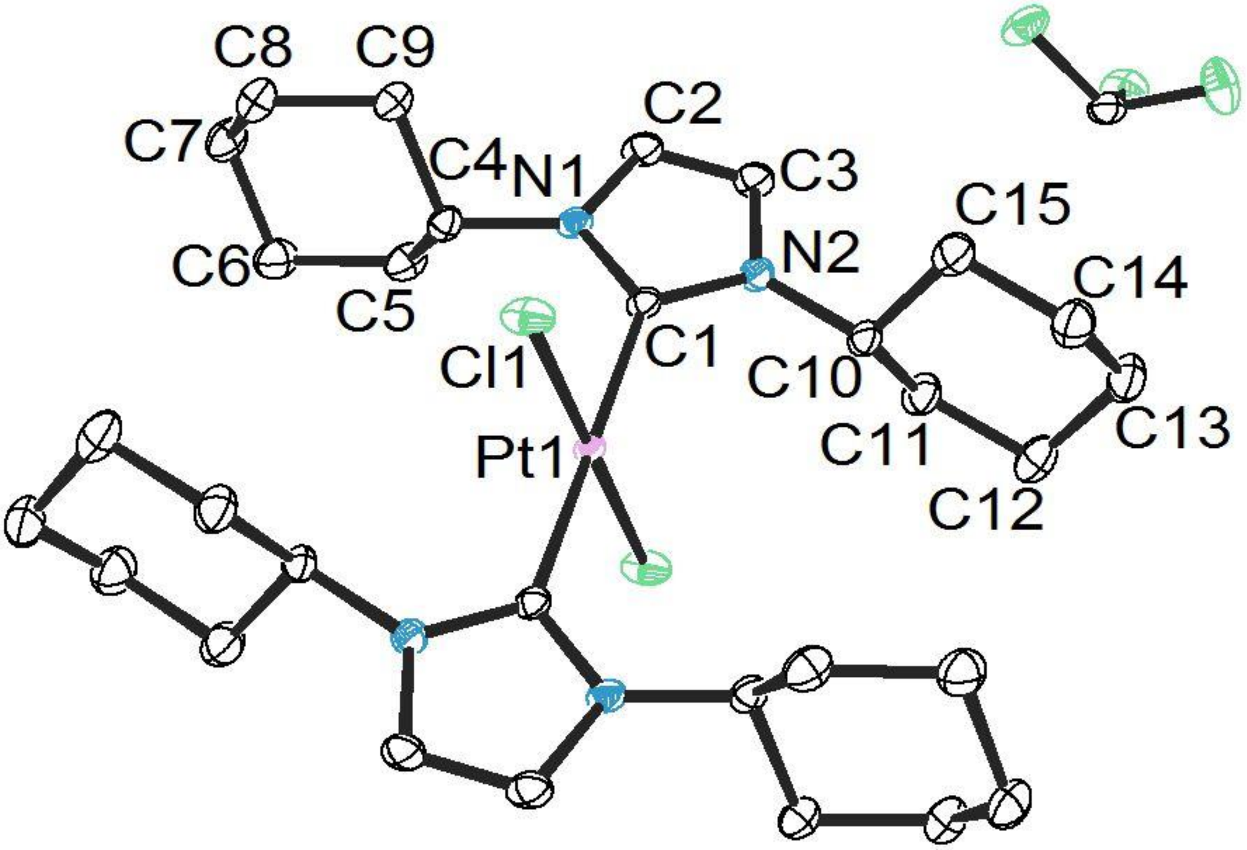

Figure 1. ORTEP diagram of *trans*-$(ICy)_2PtCl_2$ (**1**) with the asymmetric unit labeled. Ellipsoids are at the 50% probability level. Hydrogen atoms are omitted for clarity.

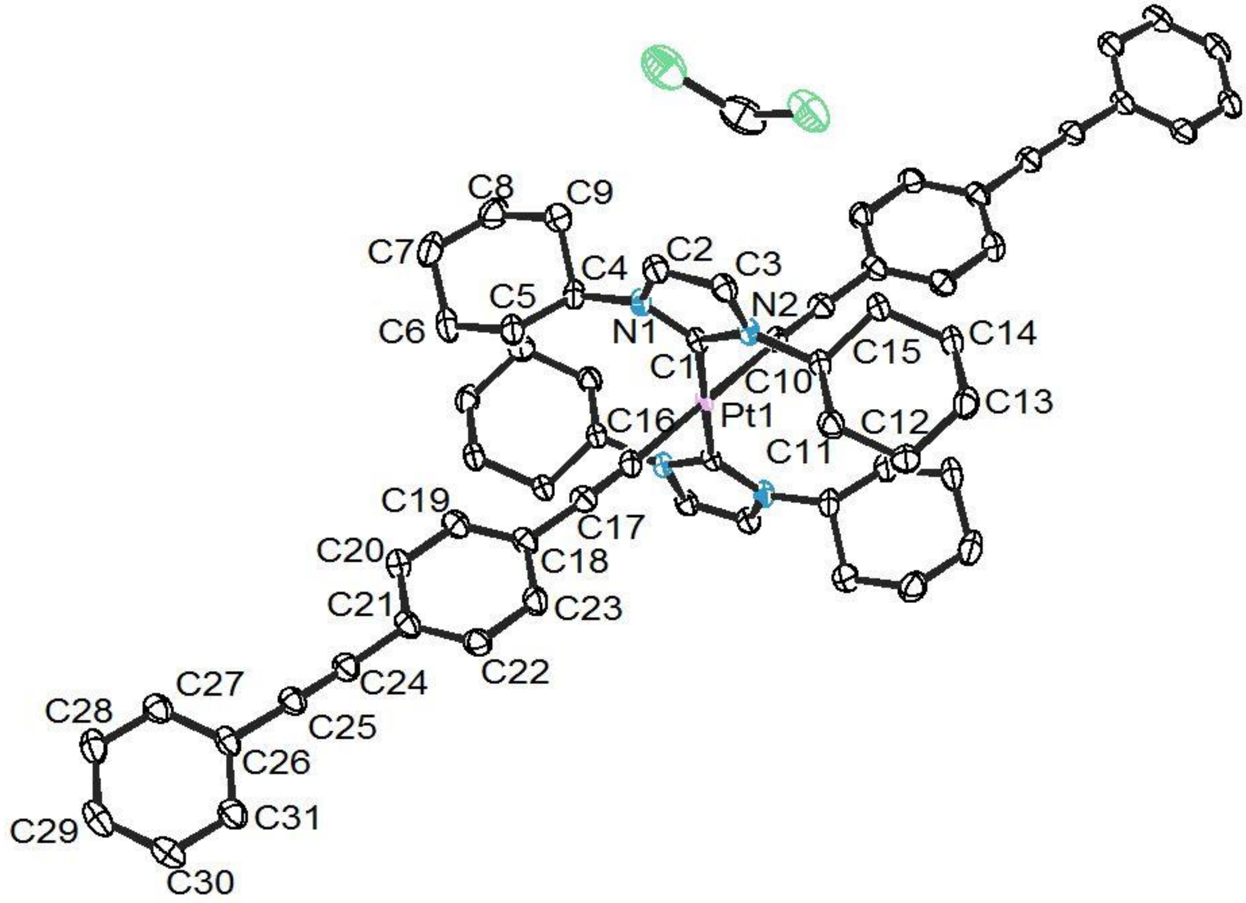

Figure 2. ORTEP diagram of *trans*-(ICy)$_2$Pt(PE2)$_2$ (**2a**) with the asymmetric unit labeled. Ellipsoids are at the 50% probability level. Hydrogen atoms are omitted for clarity.

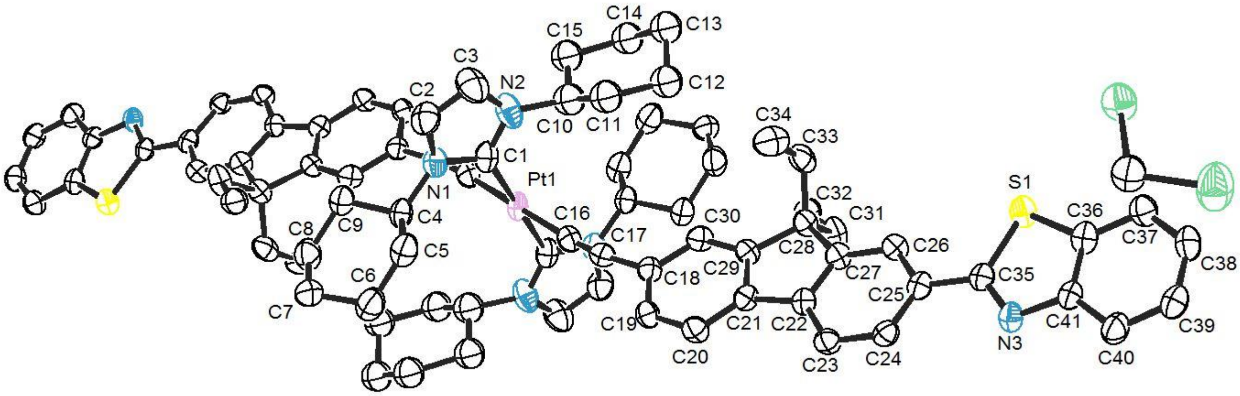

Figure 3. ORTEP diagram of *trans*-(ICy)$_2$Pt(BTF)$_2$ (**2b**) with the asymmetric unit labeled. Ellipsoids are at the 50% probability level. Hydrogen atoms are omitted for clarity.

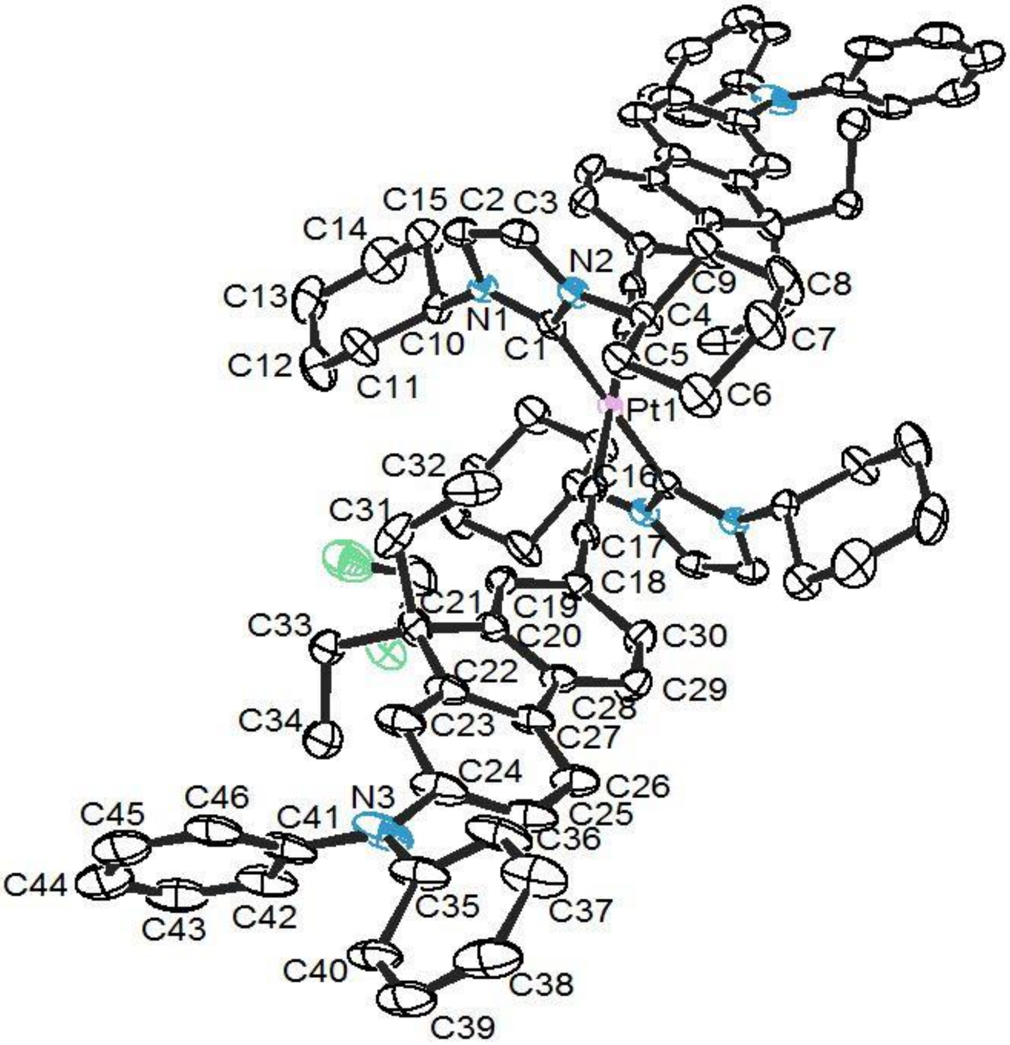

Figure 4. ORTEP diagram of *trans*-(ICy)$_2$Pt(DPAF)$_2$ (**2c**) with the asymmetric unit labeled. Ellipsoids are at the 50% probability level. Hydrogen atoms are omitted for clarity.

2. NMR Spectra

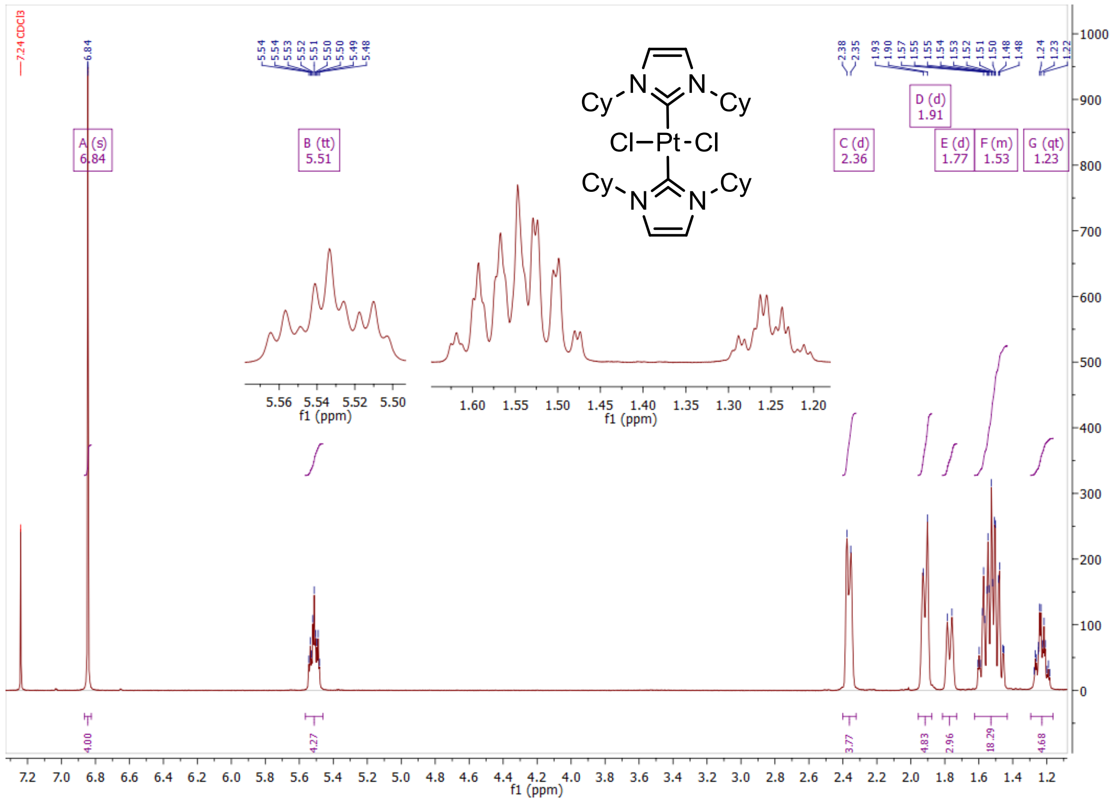

Figure 5. ^{1}H NMR (500 MHz, $CDCl_3$) of **1**

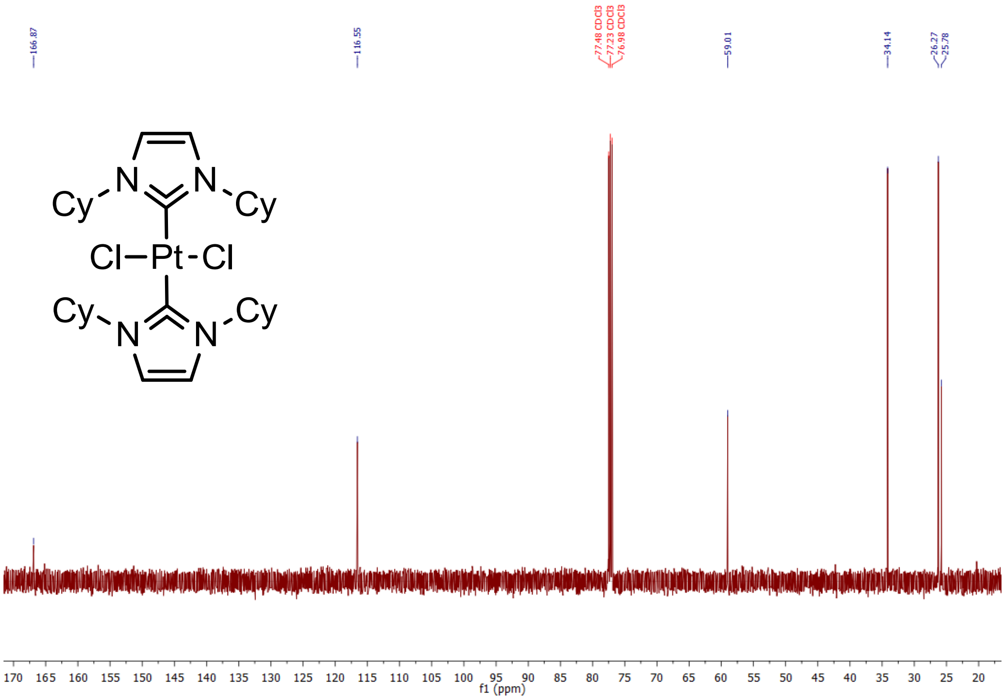

Figure 6. ^{13}C NMR (125.7 MHz, $CDCl_3$) of **1**

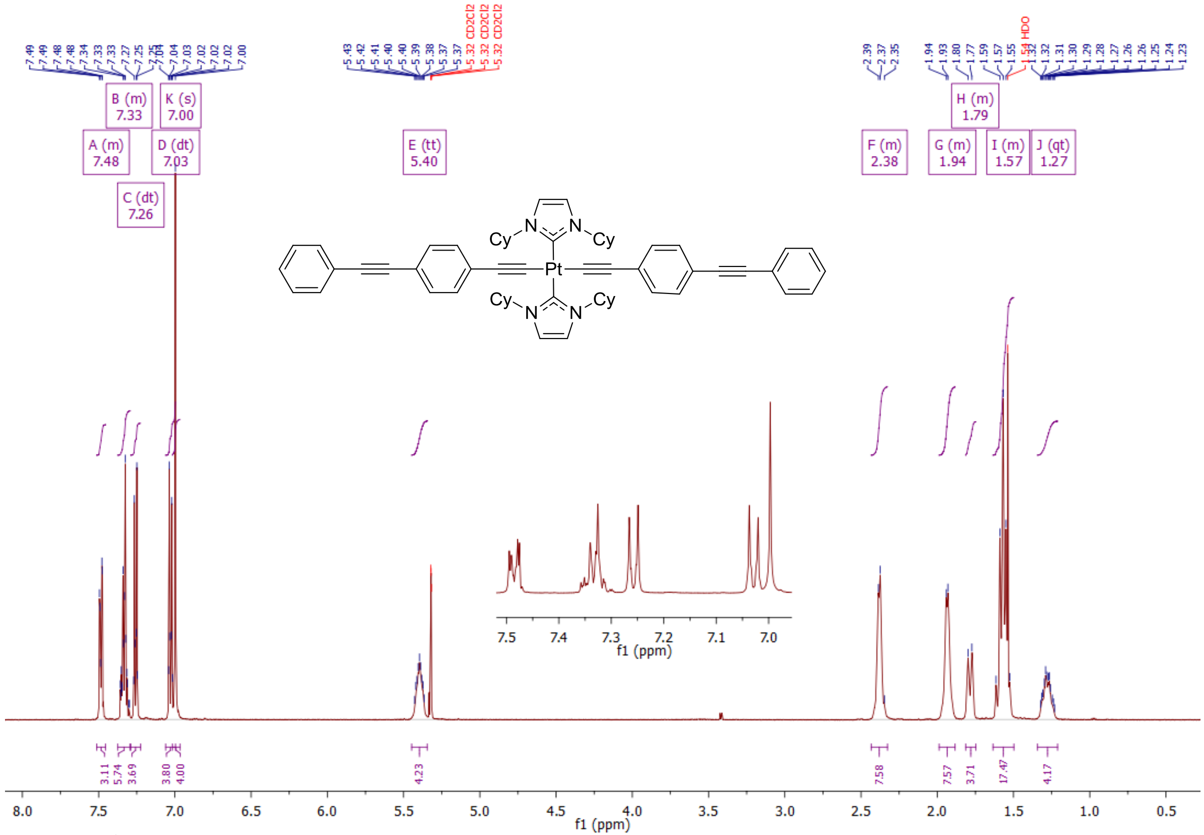

Figure 7. ^{1}H NMR (500 MHz, CD_2Cl_2) of **2a**

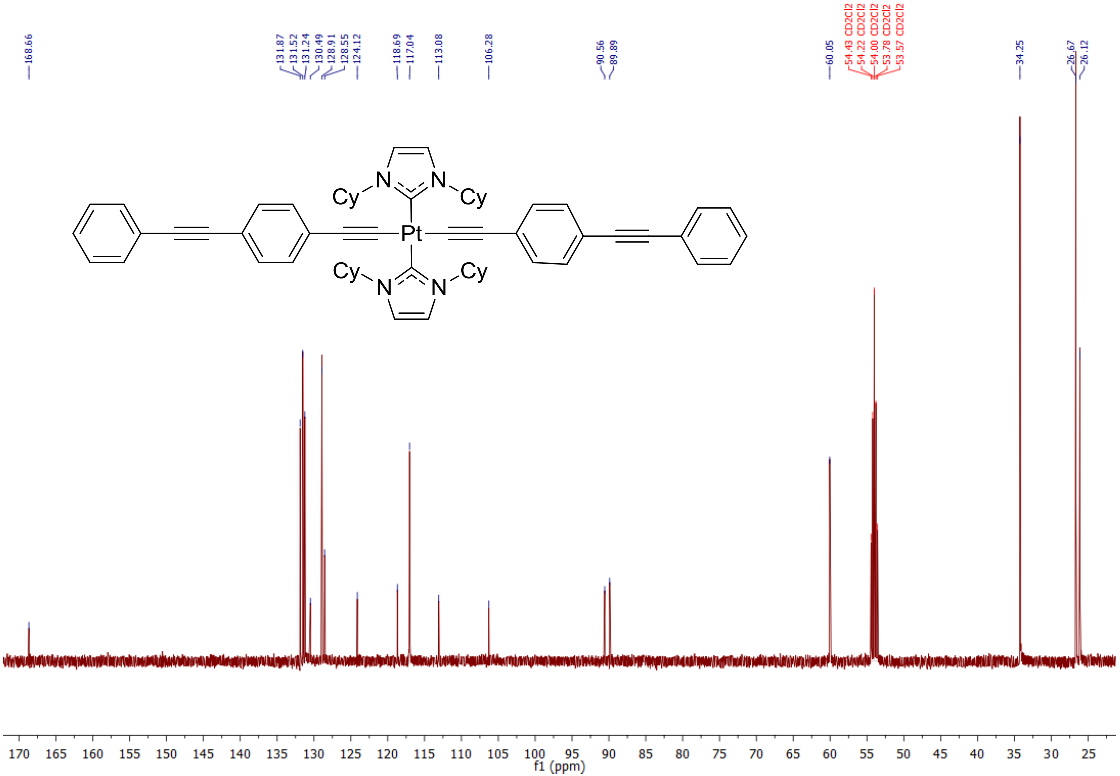

Figure 8. ^{13}C NMR (125.7 MHz, CD_2Cl_2) of **2a**

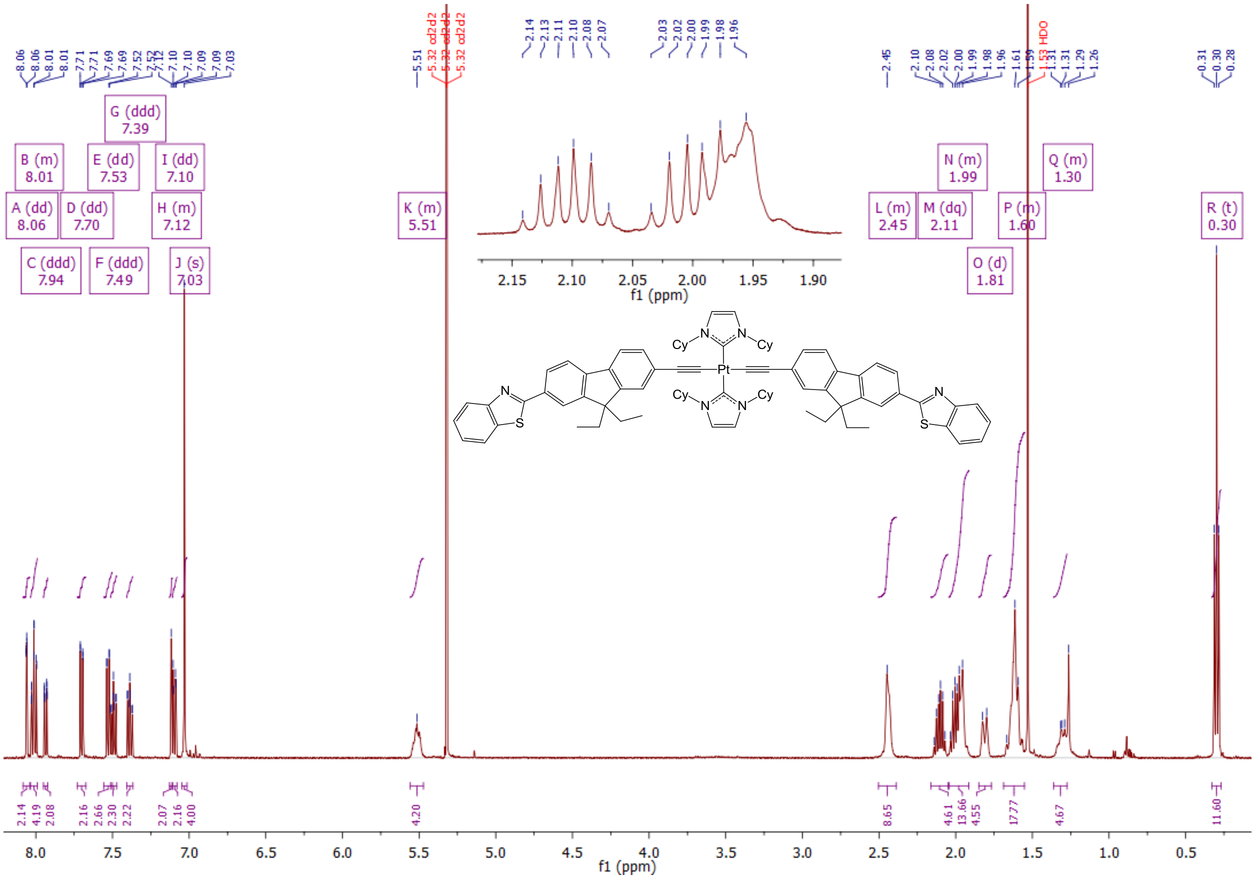

Figure 9. ^{1}H NMR (500 MHz, CD_2Cl_2) of **2b**

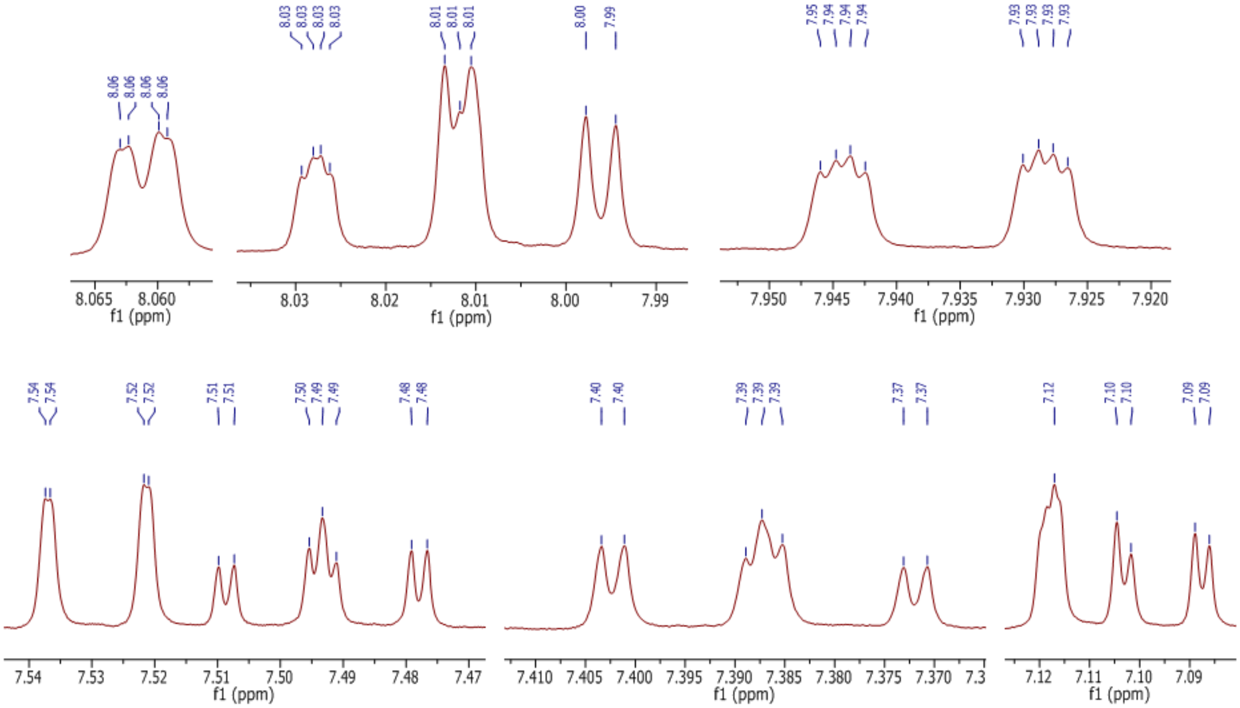

Figure 10. Insets for selected peaks from the ^{1}H NMR (500 MHz, CD_2Cl_2) of **2b**

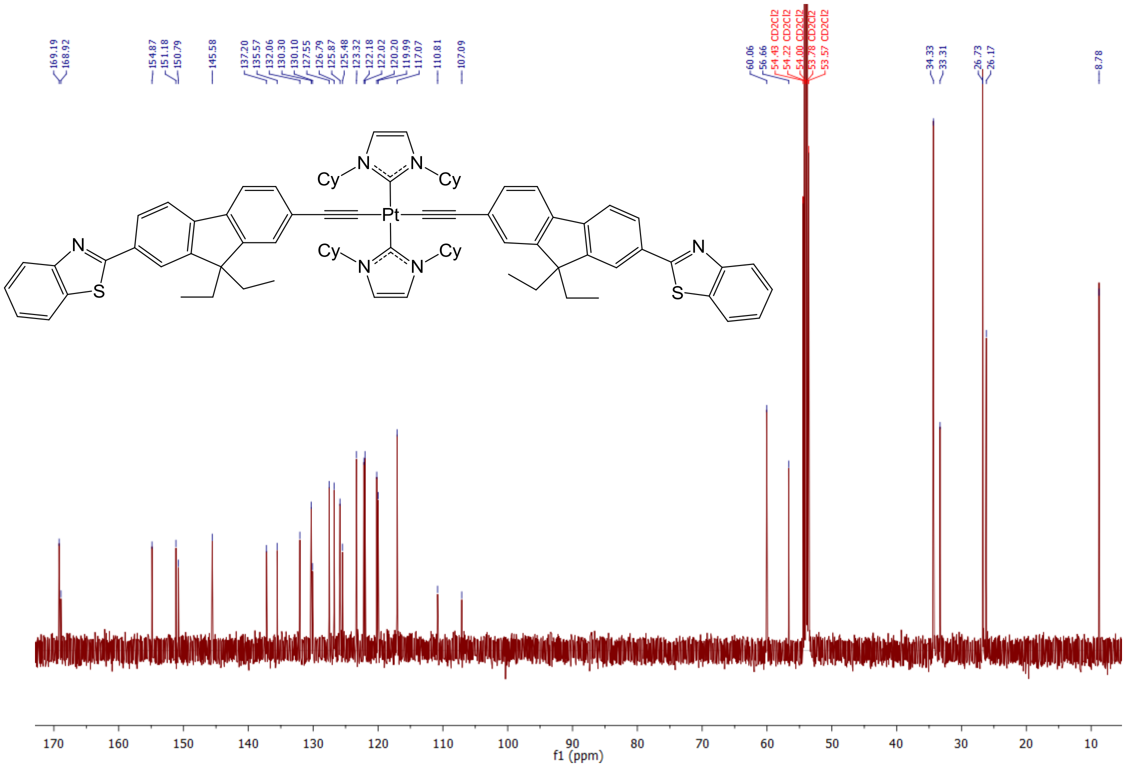

Figure 11. ^{13}C NMR (125.7 MHz, CD_2Cl_2) of **2b**

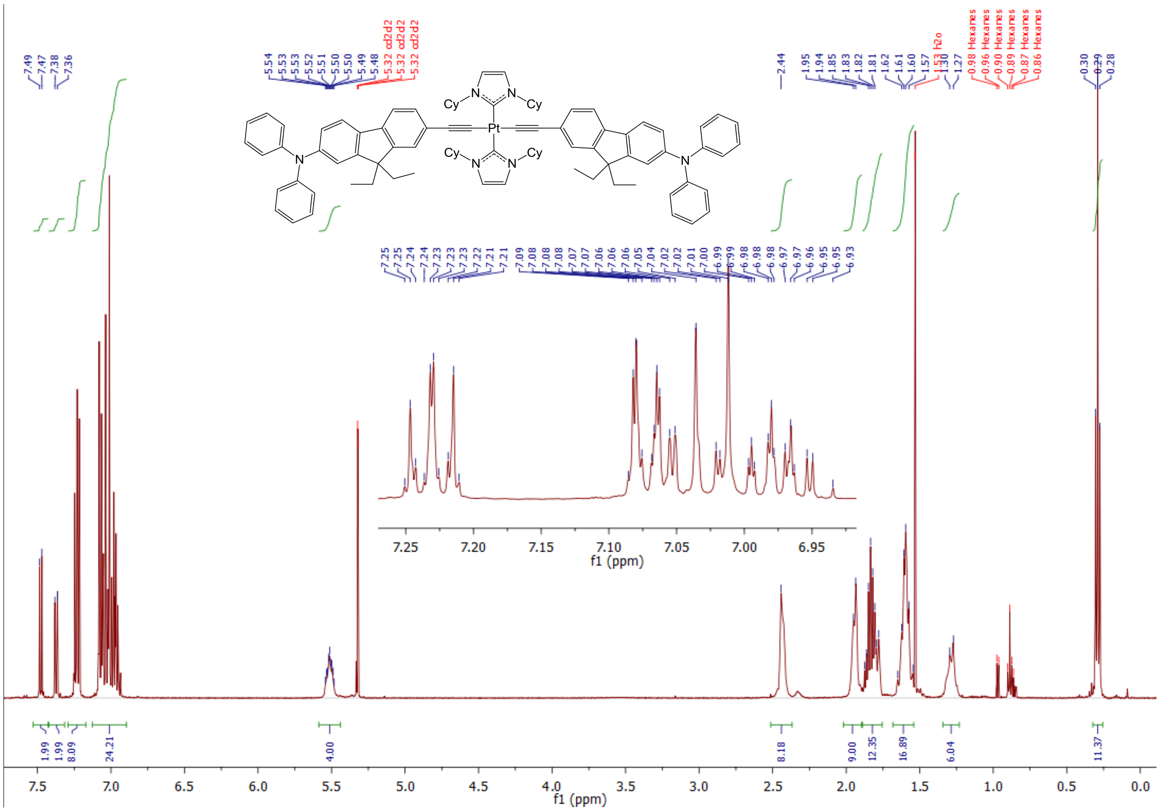

Figure 12. ^{1}H NMR (500 MHz, CD_2Cl_2) of **2c**. Residual hexanes are present.

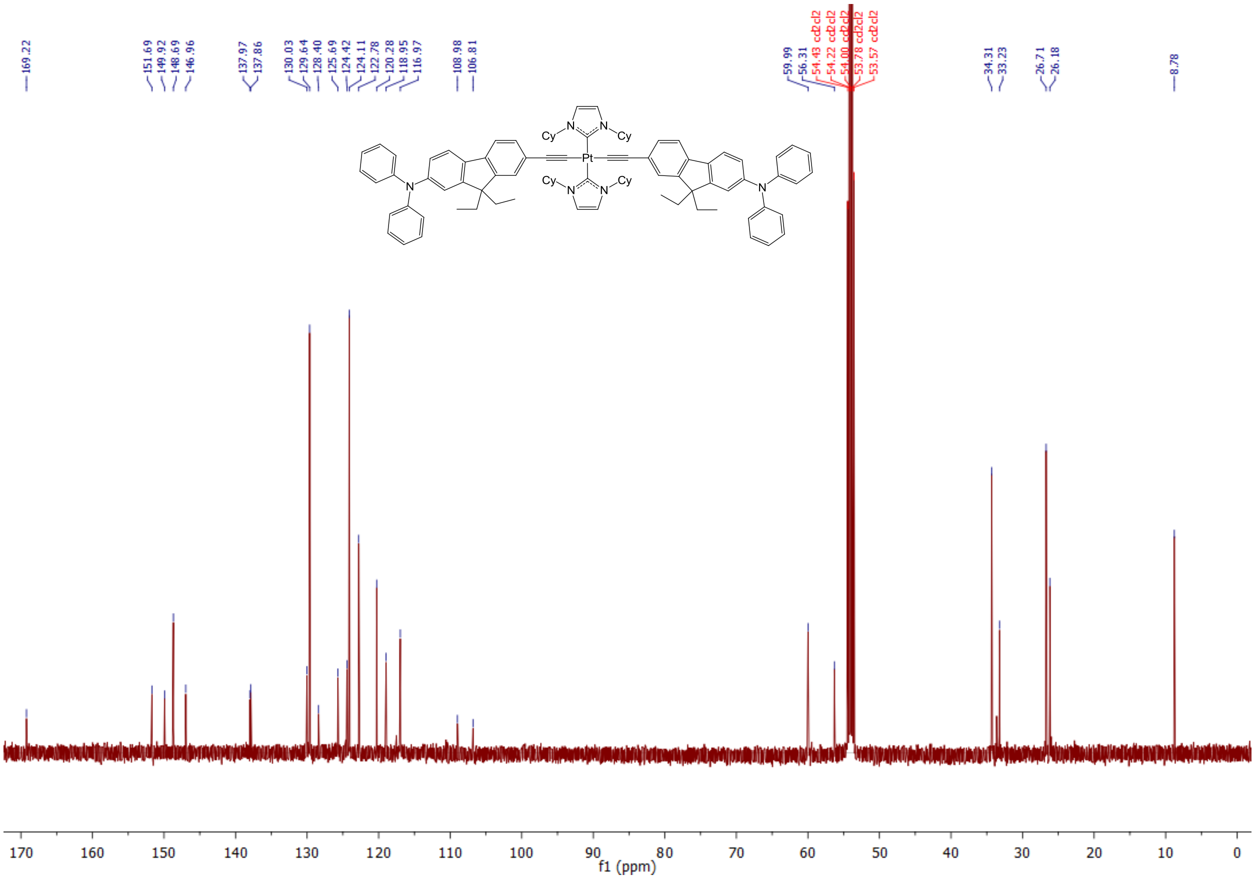

Figure 13. ^{13}C NMR (125.7 MHz, CD_2Cl_2) of **2c**.

3. IR spectra

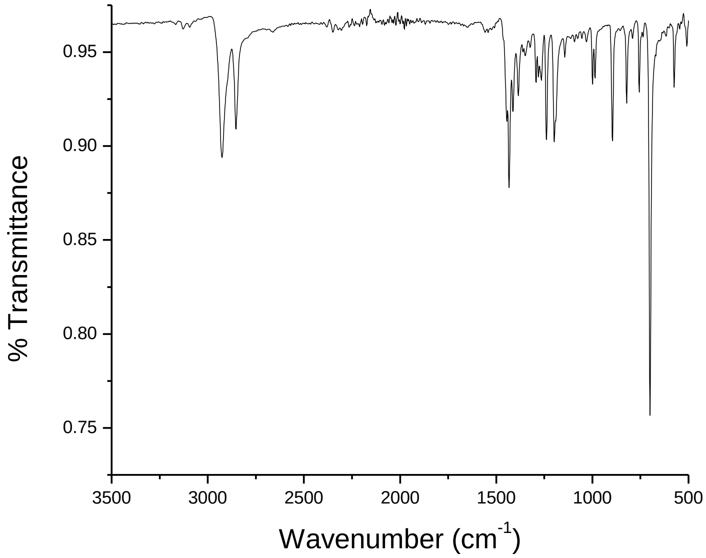

Figure 14. FTIR spectrum of **1**.

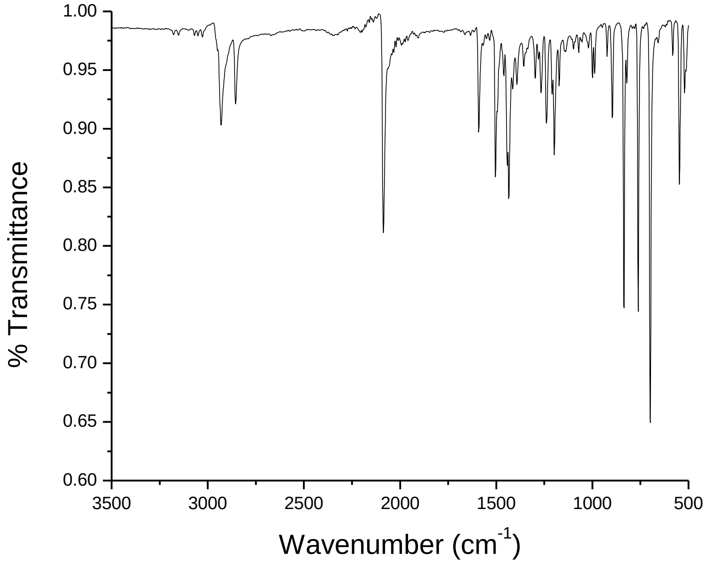

Figure 15. FTIR spectrum of **2a**.

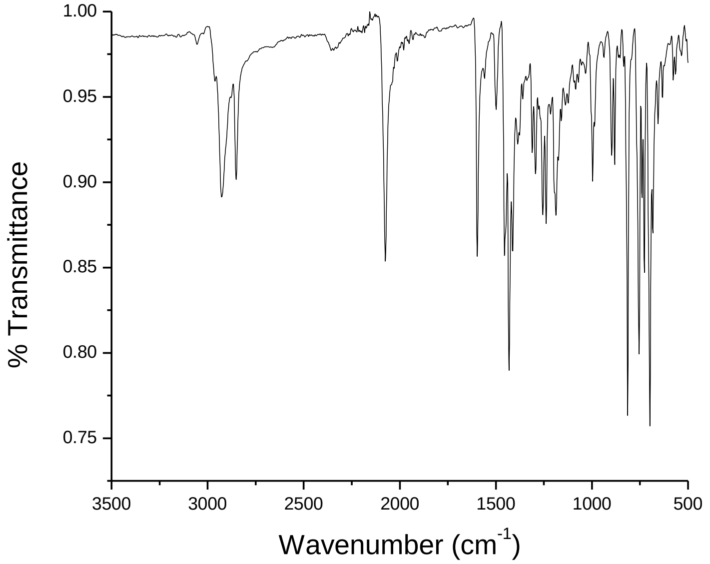

Figure 16. FTIR spectrum of **2b**.

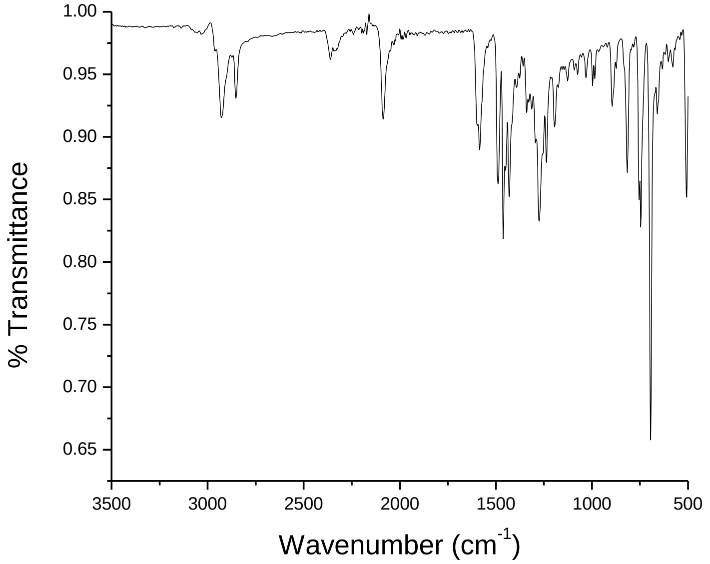

Figure 17. FTIR spectrum of **2c**.

4. Emission Lifetime Decays

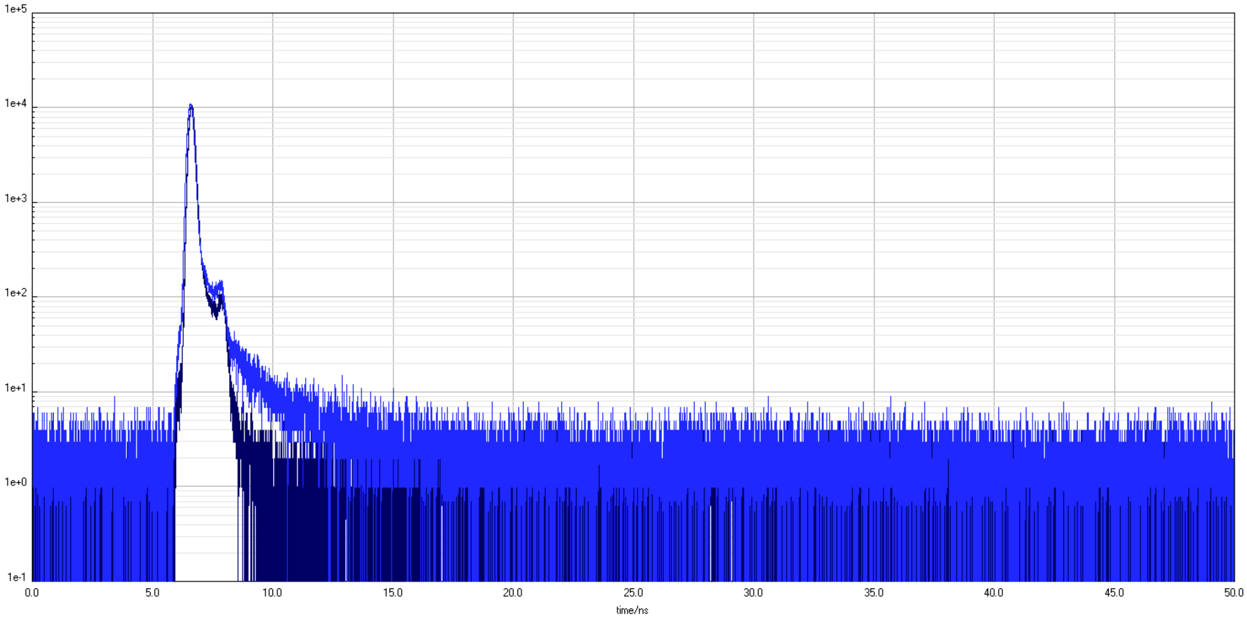

Figure 18. Fluorescence lifetime decay for **2a** (light blue) with instrument response function (dark blue).

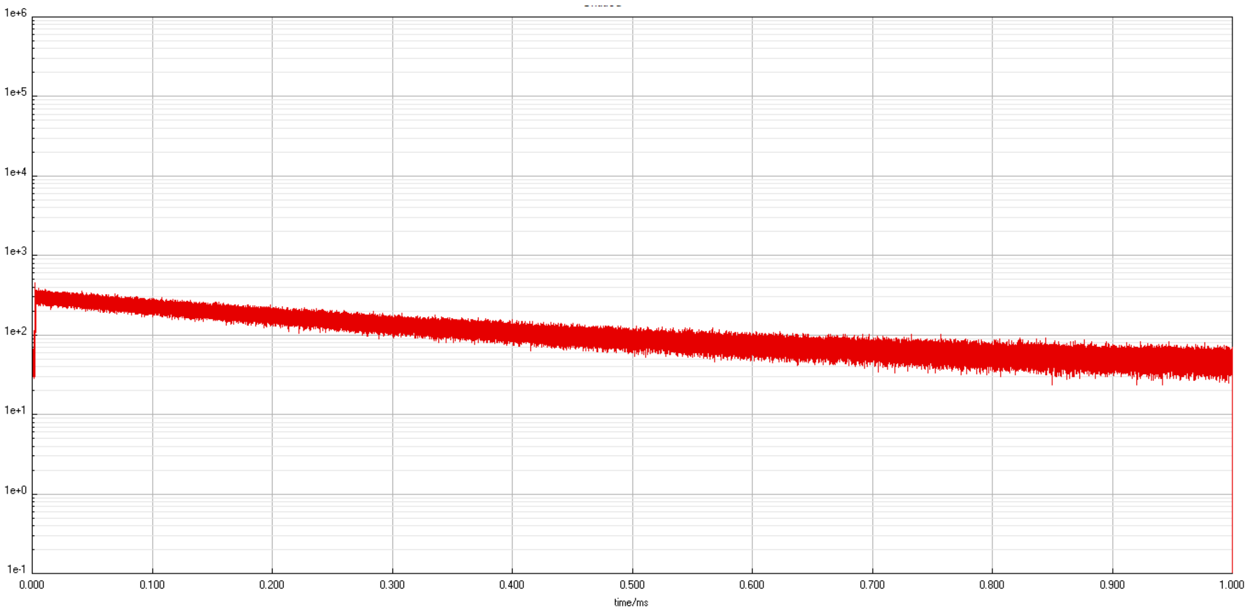

Figure 19. Phosphorescence lifetime decay for **2a**

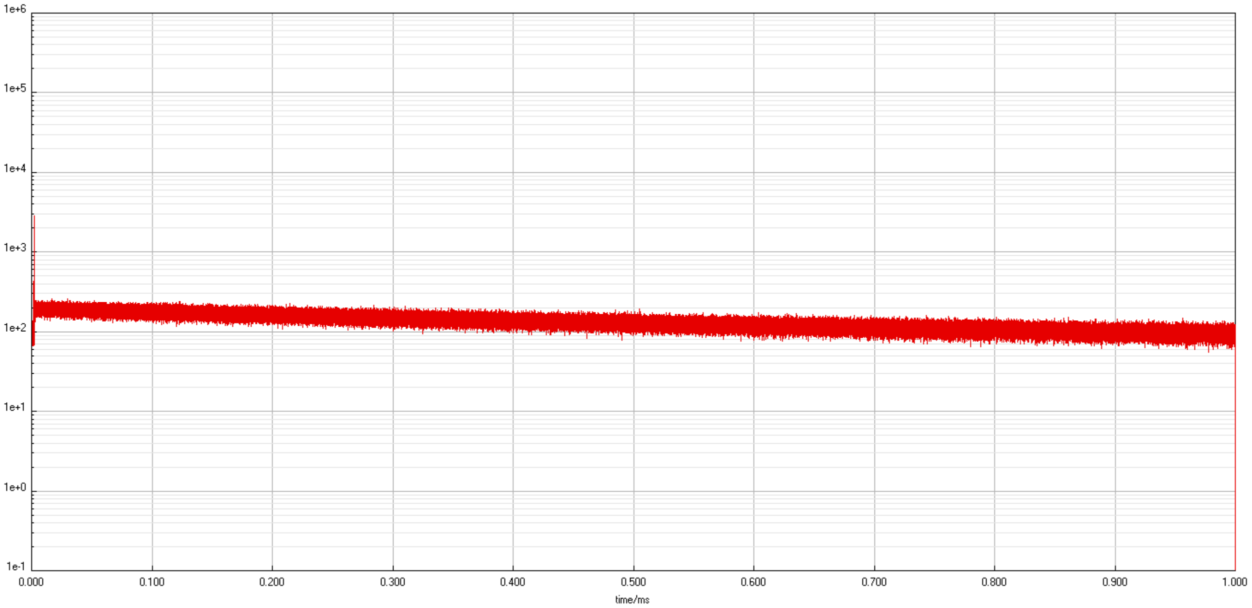

Figure 20. Phosphorescence lifetime decay for **2b**

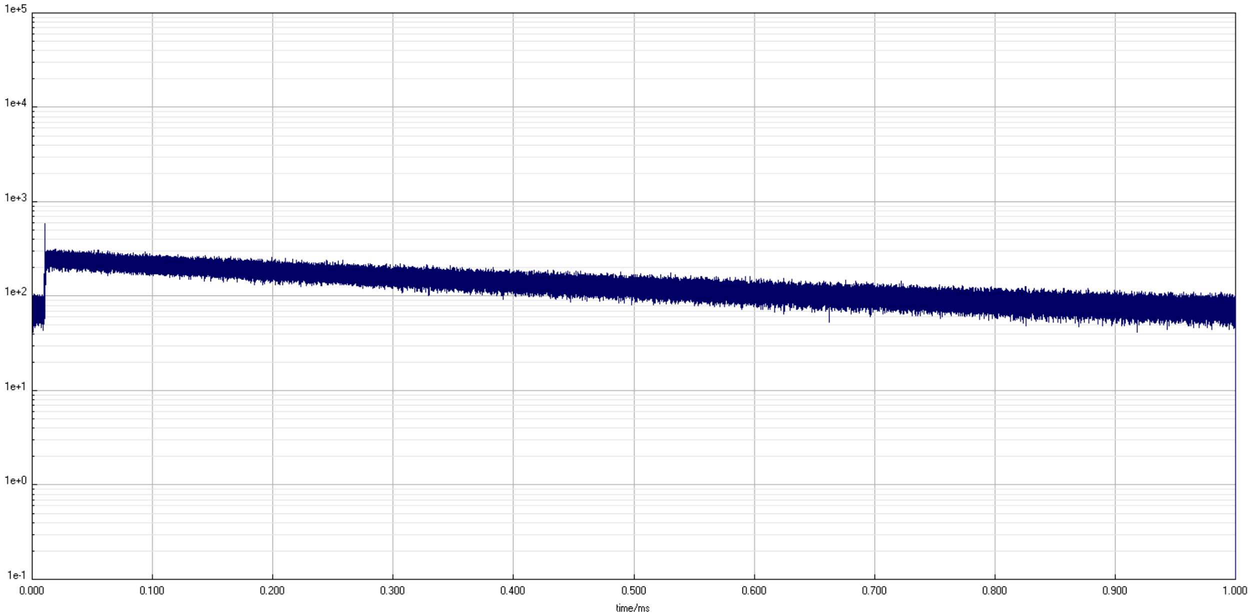

Figure 21. Phosphorescence lifetime decay for **2c**

5. Transient Absorption Decays

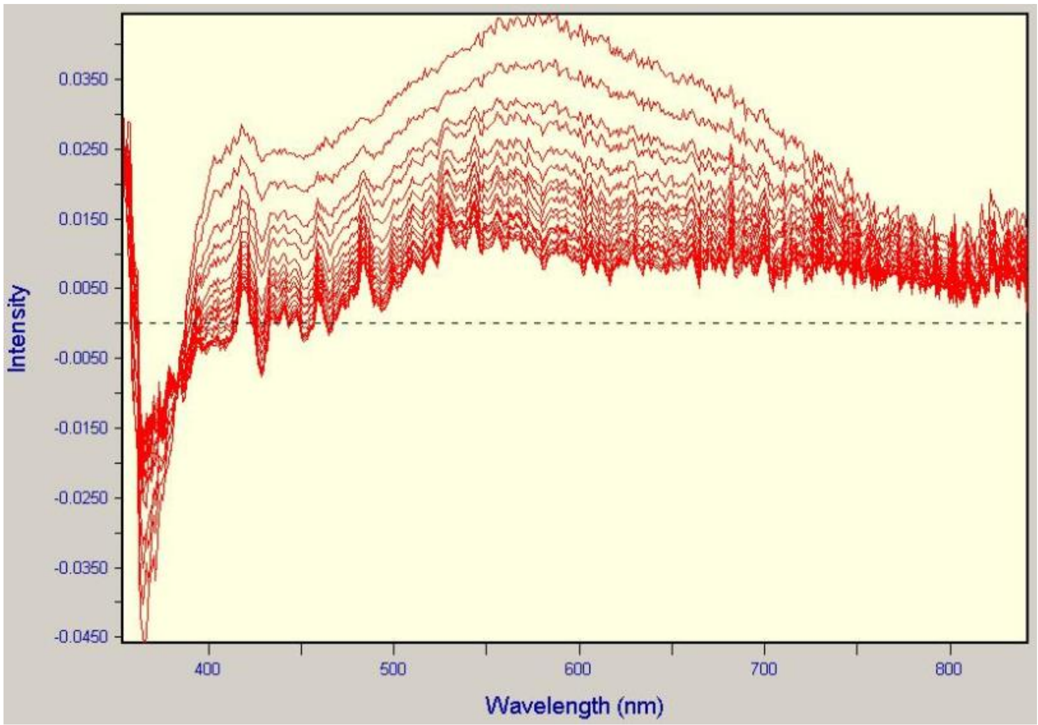

Figure 22. Transient absorption decay for **2a**. Initial camera delay: 100ns, camera delay increment: 15 µs, 100 images averaged per trace, Q-switch delay: 380 µs, 180 µJ per pulse.

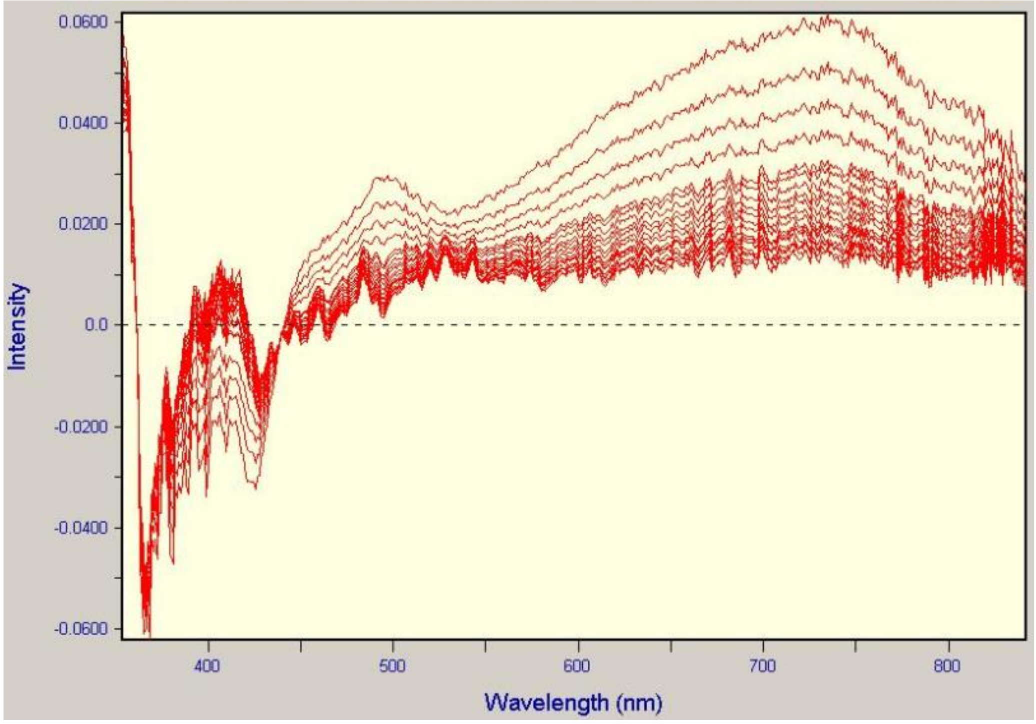

Figure 23. Transient absorption decay for **2b**. Initial camera delay: 100ns, camera delay increment: 20 µs, 100 images averaged per trace, Q-switch delay: 382 µs, 180 µJ per pulse.

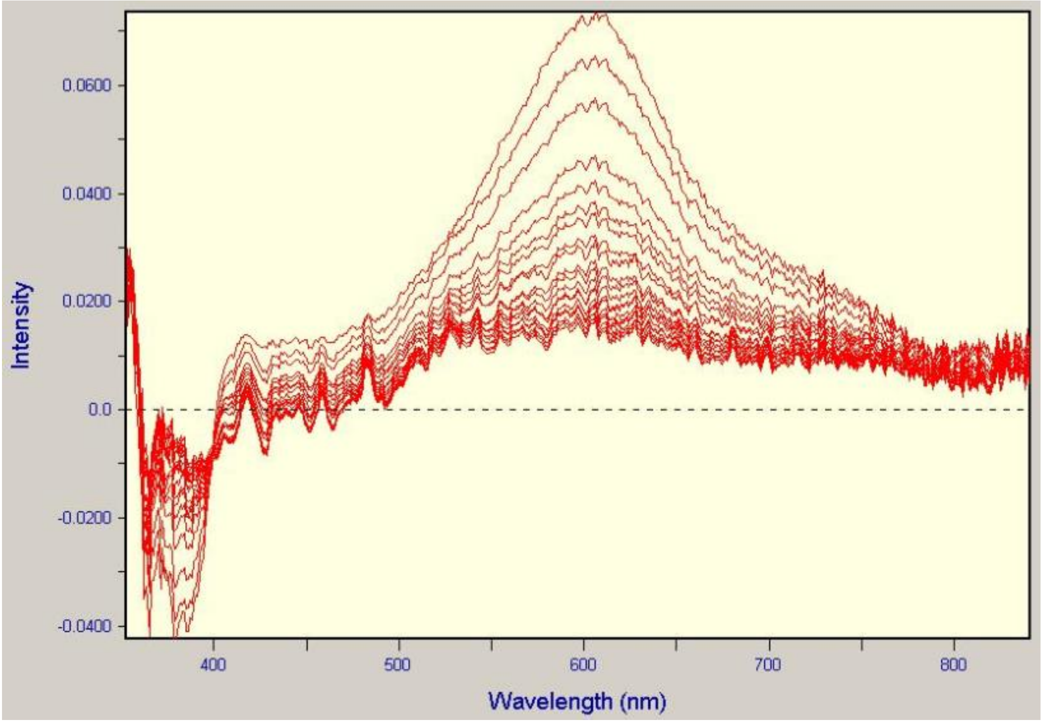

Figure 24. Transient absorption decay for **2c**. Initial camera delay: 100ns, camera delay increment: 20 µs, 100 images averaged per trace, Q-switch delay: 379 µs, 180 µJ per pulse.

6. Triplet-Triplet Absorption Power Dependence

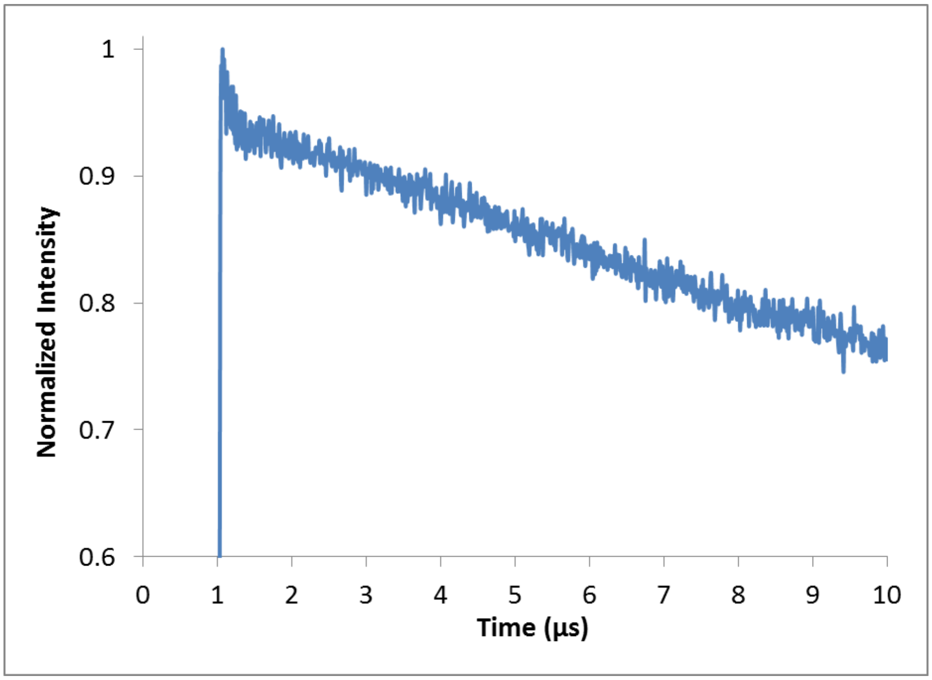

Figure 25. Transient absorption decay profile for **2a**. Conditions: 200 µJ per pulse, 380 µJ Q-switch delay, 128 scans averaged, decay measured at 584 nm.

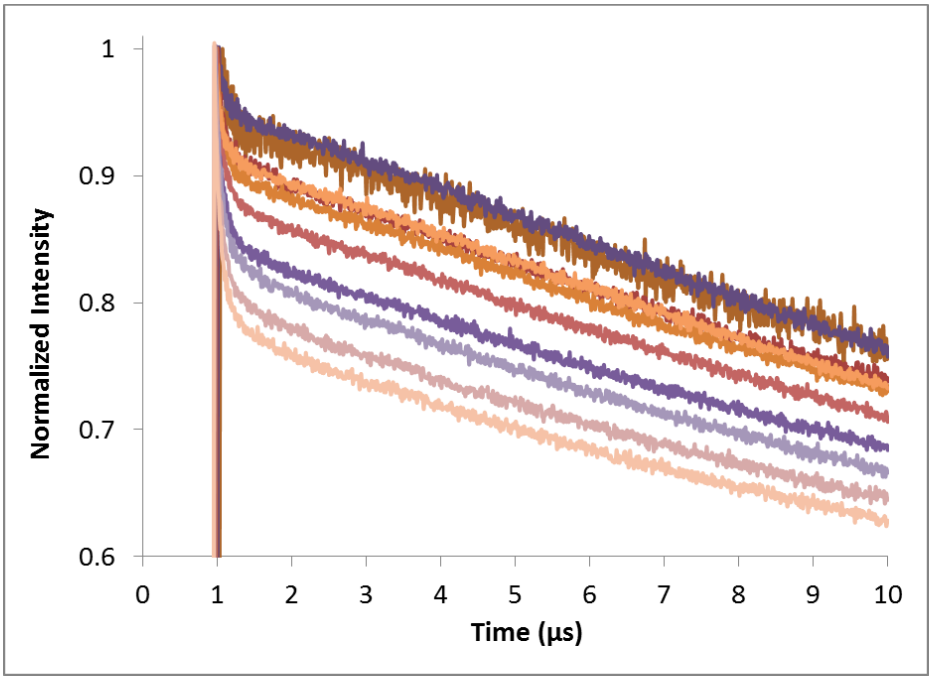

Figure 26. Transient absorption decay profiles for **2a** at varying laser energies. Conditions: 200 µJ – 18 mJ per pulse, 380-200 µJ Q-switch delay, 128 scans averaged per trace, decays measured at 584 nm.

7. Computational Studies

DFT and TD-DFT calculations were performed in the Gaussian 09, revision C.01, suite of programs at the B3LYP level with the 6-31G(d) basis set for nonmetals and the SDD basis set for Pt. Carbene cyclohexane groups were replaced by methyl groups to improve computational efficiency. These truncated complexes are denoted as **2a'-c'**. The ground state structures were optimized in the gas phase from idealized starting configurations without symmetry constraints. The optimized structures were confirmed to be minima by the lack of negative modes in a frequency calculation. Structures and orbitals were visualized using Chemcraft Version 1.7, which was also used to generate charge difference density (CDD) plots. Orbitals were visualized at an isosurface value of 0.02, while CDDs were visualized at an isosurface value of 0.0004.

Table 2. Summary of TD-DFT Computations for Vertical Excitations of Oscillator Strength Greater than 0.1 for Compounds **2a'-c'**.

Complex	Root	Wavelength (nm)	Orbital Transitions (% contribution)		Oscillator Strength, *f*
2a'	1	373.8	165→168 HOMO-1 → LUMO+1 166→167 HOMO → LUMO	(2.4%) (97.6%)	2.3830
	6	334.2	165→168 HOMO-1 → LUMO+1 166→167 HOMO → LUMO	(97.3%) (2.7%)	1.0319
2b'	1	429.3	259→262 HOMO-1 → LUMO+1 260→261 HOMO → LUMO	(5.3%) (94.7%)	2.2796
	4	381.6	258→261 HOMO-2 → LUMO 259→262 HOMO-1 → LUMO+1 260→261 HOMO → LUMO	(13.7%) (81.8%) (4.5%)	0.7184
	8	316.4	256→262 HOMO-4 → LUMO+1 257→261 HOMO-3 → LUMO 260→265 HOMO → LUMO+4	(14.7%) (75.6%) (9.7%)	0.7139
2c'	1	381.5	279→282 HOMO-1 → LUMO+1 280→281 HOMO → LUMO	(18.3%) (81.7%)	2.6813
	4	344.6	278→281 HOMO-2 → LUMO 279→282 HOMO-1 → LUMO+1 280→281 HOMO → LUMO	(3.6%) (77.8%) (18.6%)	0.1267
	10	319.53	278→286 HOMO-2 → LUMO+5 279→286 HOMO-1 → LUMO+5 279→287 HOMO-1 → LUMO+6 280→286 HOMO → LUMO+5	(2.3%) (24.3%) (12.9%) (60.5%)	0.1648
	11	319.50	278→287 HOMO-2 → LUMO+6 279→286 HOMO-1 → LUMO+5 279→287 HOMO-1 → LUMO+6 280→287 HOMO → LUMO+6	(2.2%) (13.1%) (24.4%) (60.3%)	0.1494
	12	315.3	276→282 HOMO-4 → LUMO+1 278→281 HOMO-2 → LUMO 279→282 HOMO-1 → LUMO+1	(11.1%) (85.7%) (3.2%)	0.2115

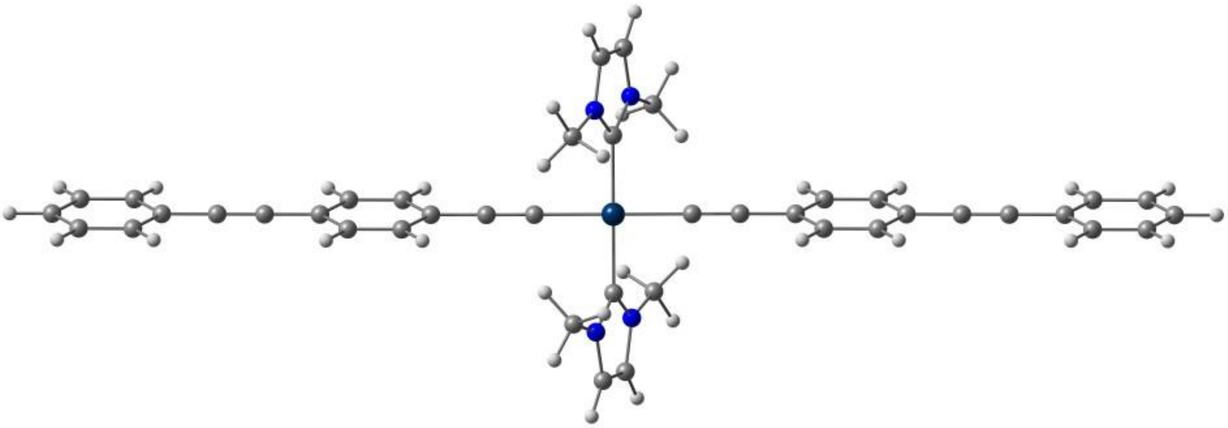

Figure 27. DFT optimized structure of **2a**.

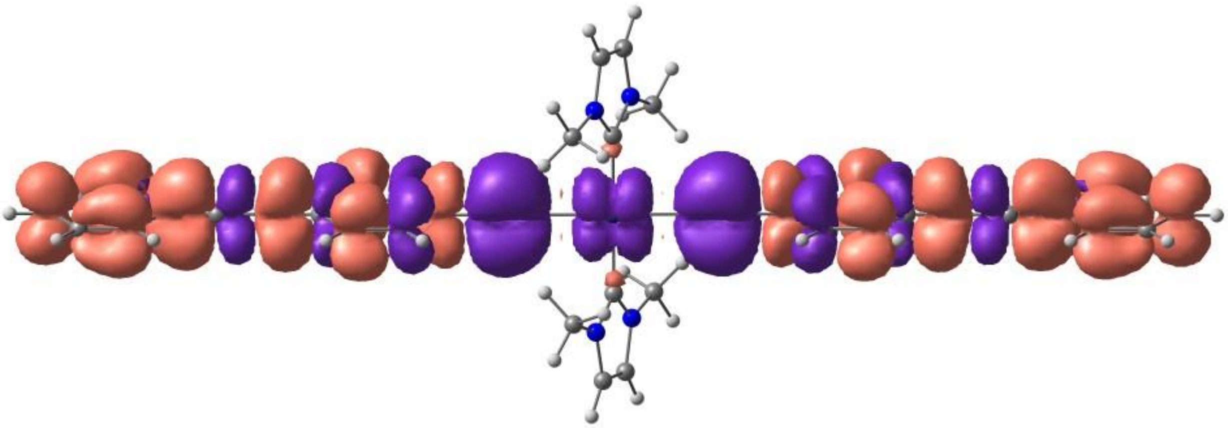

Figure 28. 373.8 nm CDD of **2a**. Blue coloring indicates electron density being lost, while red coloring indicates electron density being gained in the electronic transition.

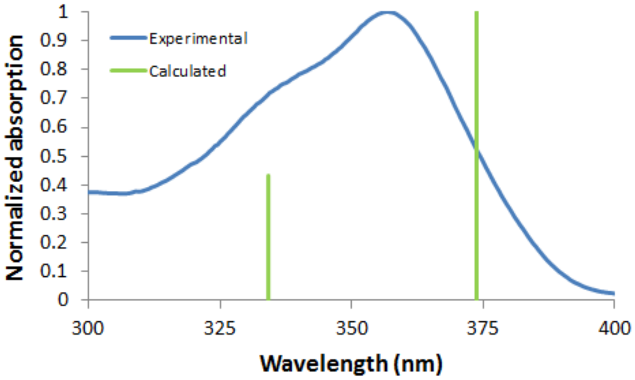

Figure 29. Normalized overlay of the experimental absorption spectrum of **2a** with the TDDFT computed line spectra of **2a'**. Only vertical excitations with $f > 0.1$ are shown.

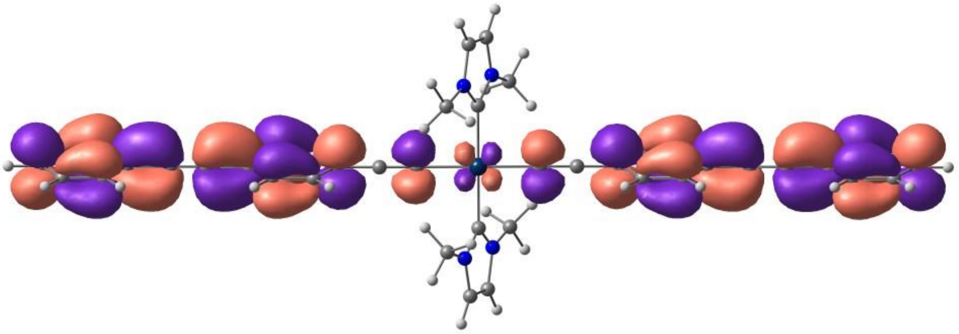

Figure 30. LUMO+1 (orbital 168) of compound **2a**.

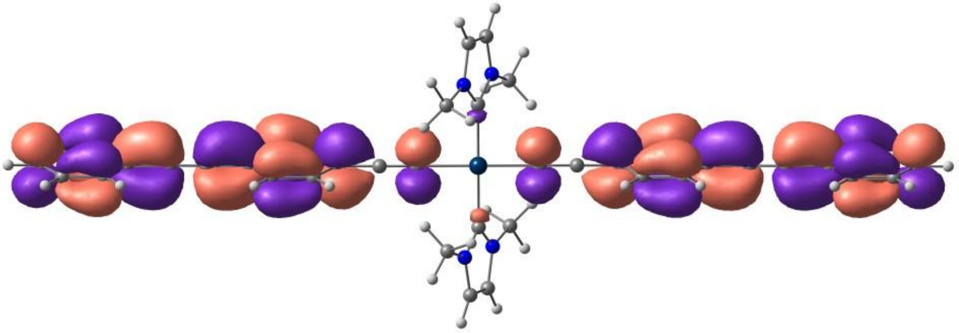

Figure 31. LUMO (orbital 167) of compound **2a**.

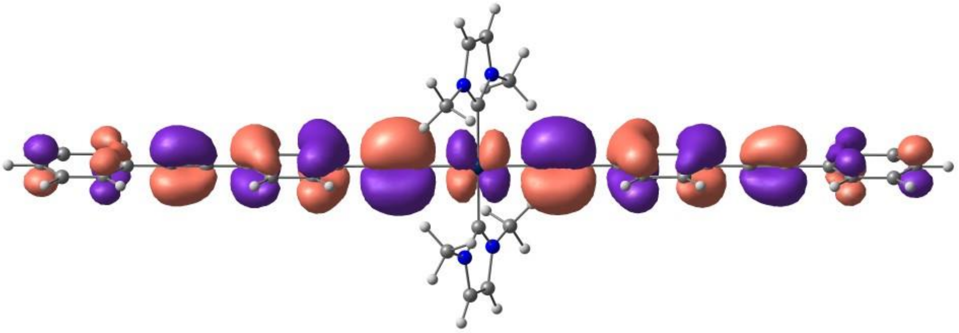

Figure 32. HOMO (orbital 166) of compound **2a**.

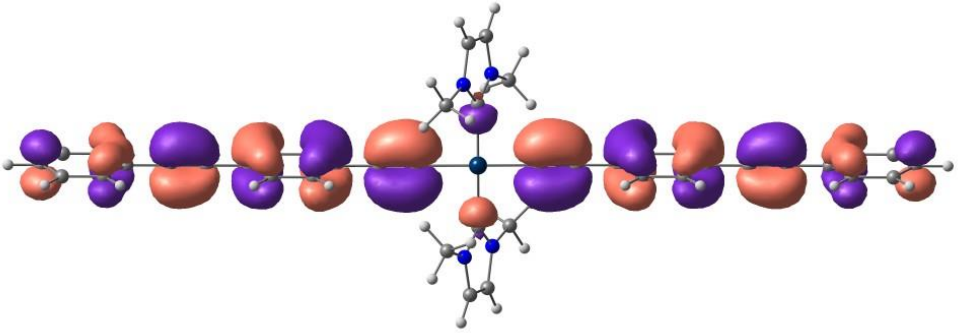

Figure 33. HOMO-1 (orbital 165) of compound **2a**.

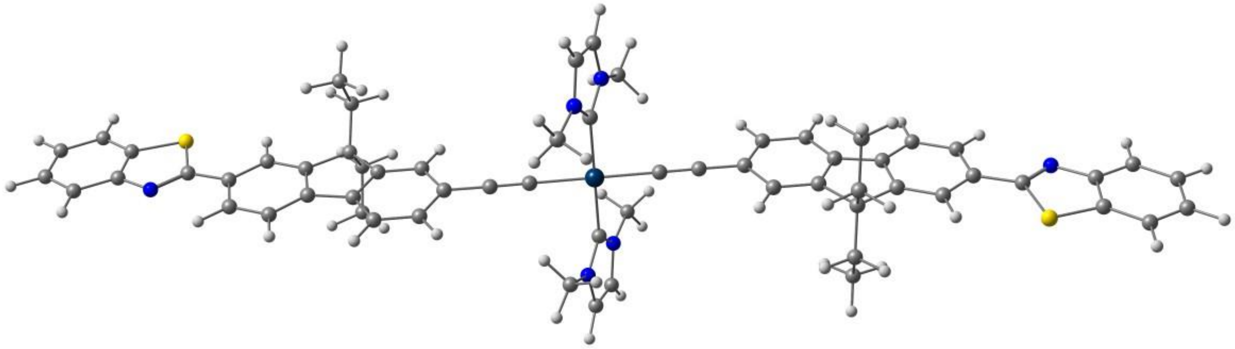

Figure 34. DFT optimized structure of **2b**.

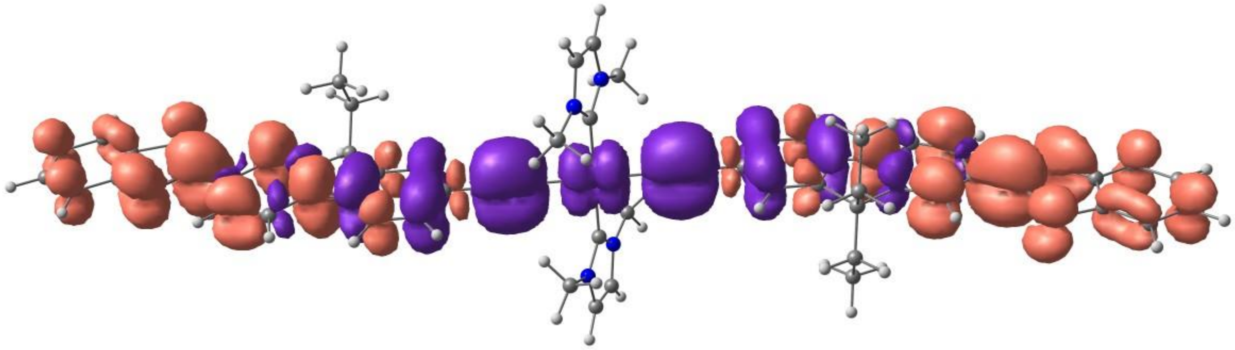

Figure 35. 429.3 nm CDD of **2b**. Blue coloring indicates electron density being lost, while red coloring indicates electron density being gained in the electronic transition.

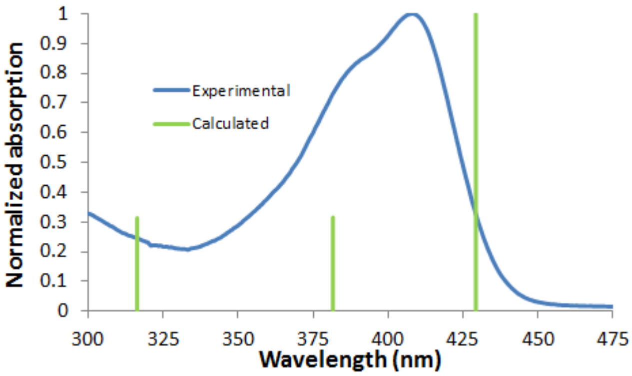

Figure 36. Normalized overlay of the experimental absorption spectrum of **2b** with the TDDFT computed line spectra of **2b'**. Only vertical excitations with $f > 0.1$ are shown.

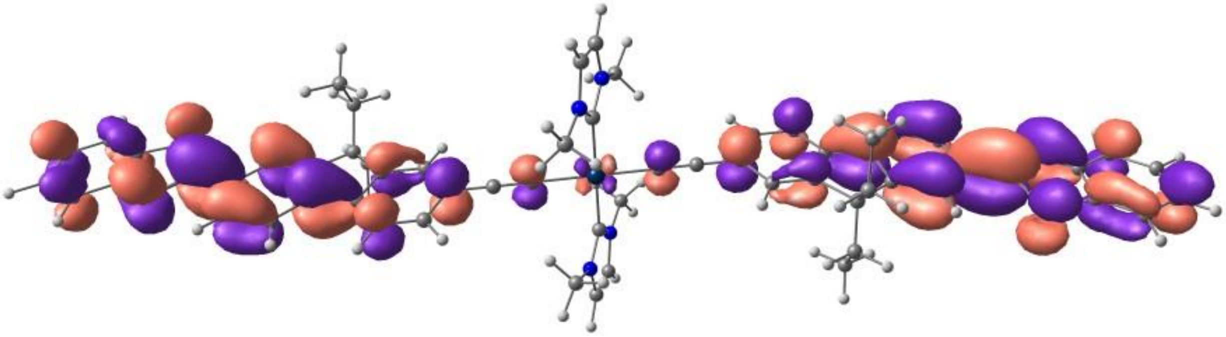

Figure 37. LUMO+1 (orbital 262) of compound **2b**.

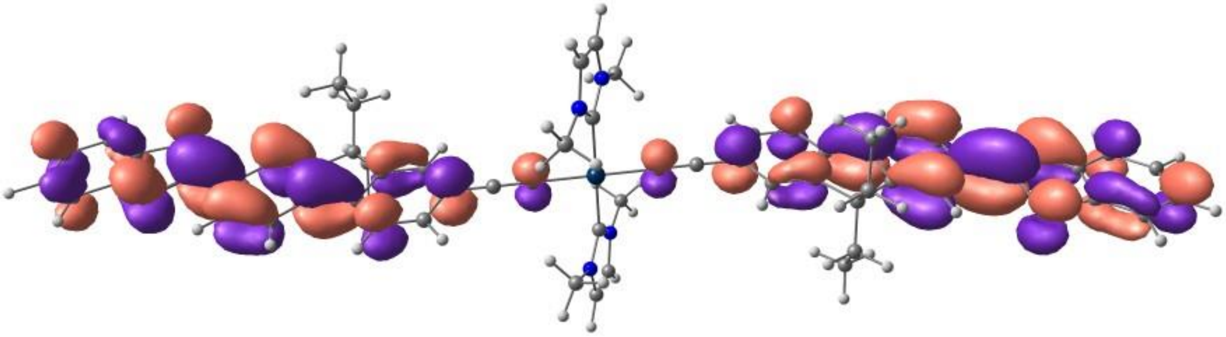

Figure 38. LUMO (orbital 261) of compound **2b**.

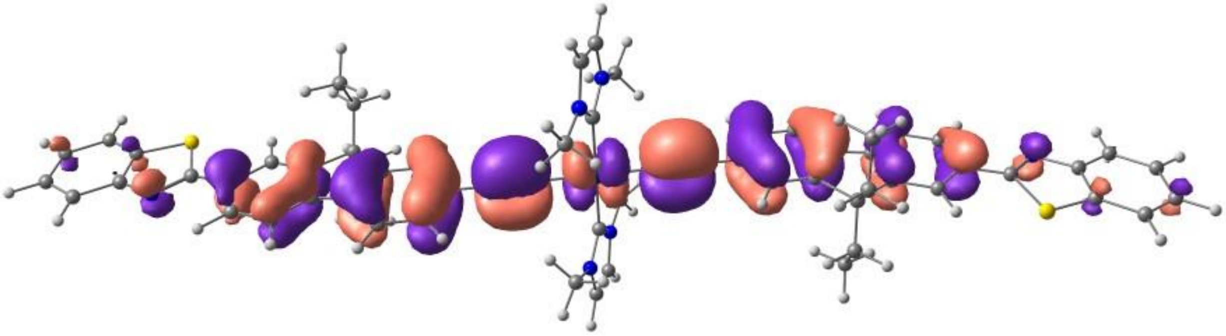

Figure 39. HOMO (orbital 260) of compound **2b**.

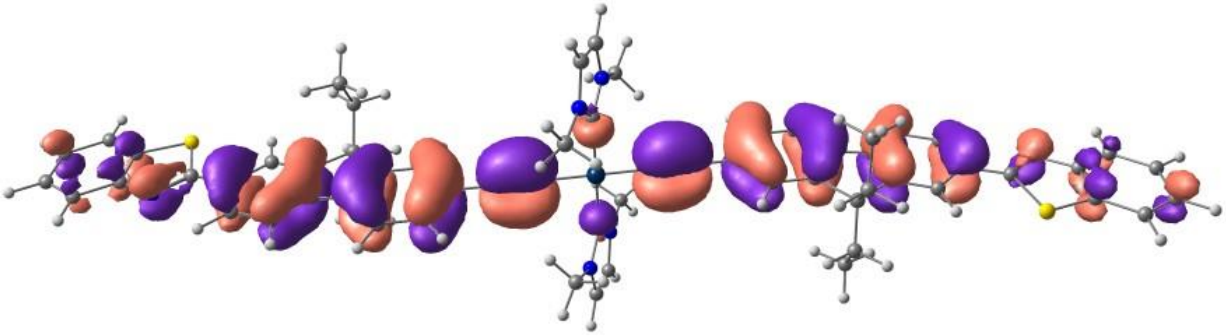

Figure 40. HOMO-1 (orbital 259) of compound **2b**.

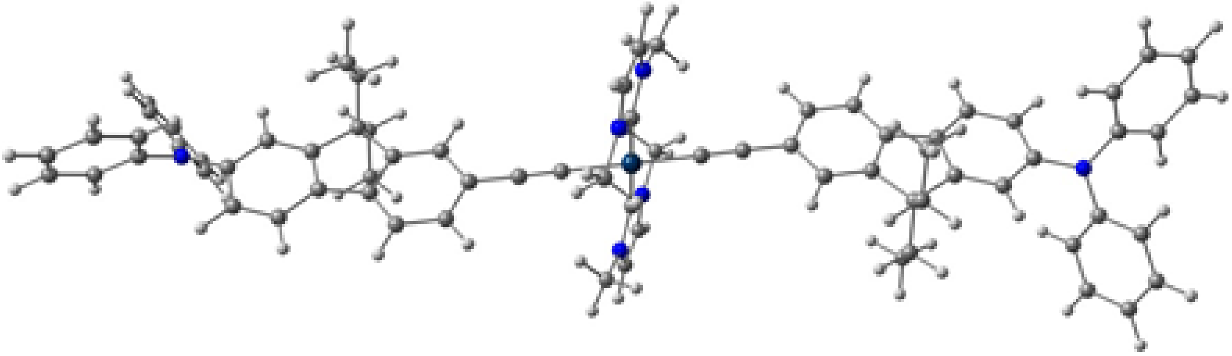

Figure 41. DFT optimized structure of **2c**.

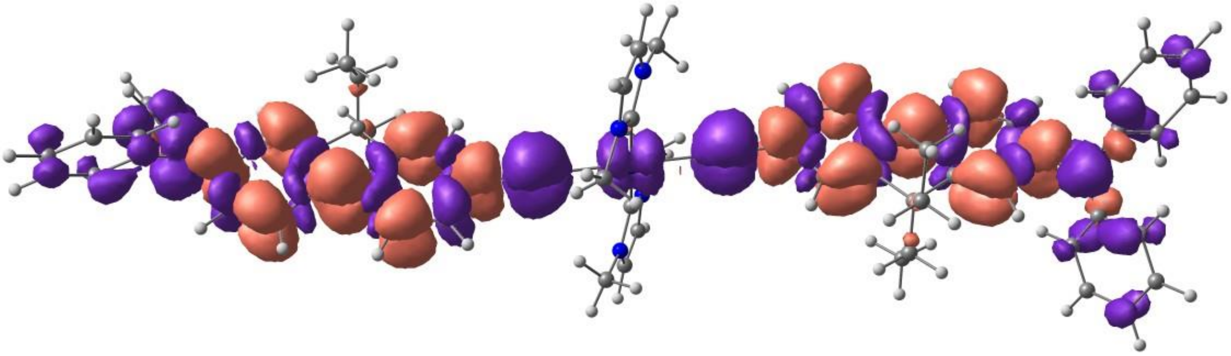

Figure 42. 381.5 nm CDD of **2c**. Blue coloring indicates electron density being lost, while red coloring indicates electron density being gained in the electronic transition.

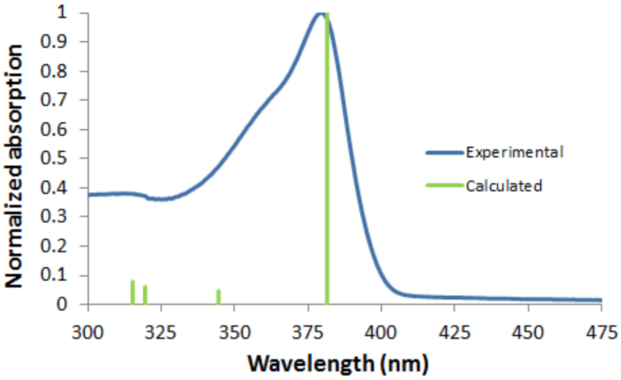

Figure 43. Normalized overlay of the experimental absorption spectrum of **2c** with the TDDFT computed line spectra of **2c’**. Only vertical excitations with $f > 0.1$ are shown.

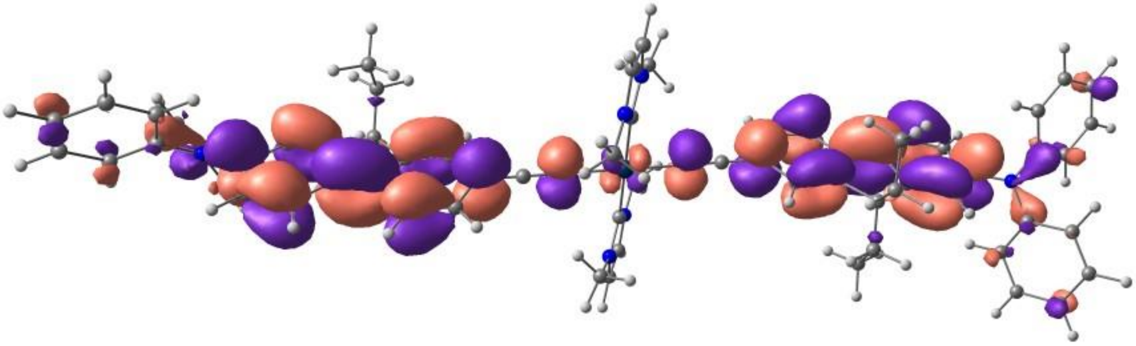

Figure 44. LUMO+1 (orbital 282) of compound **2c**.

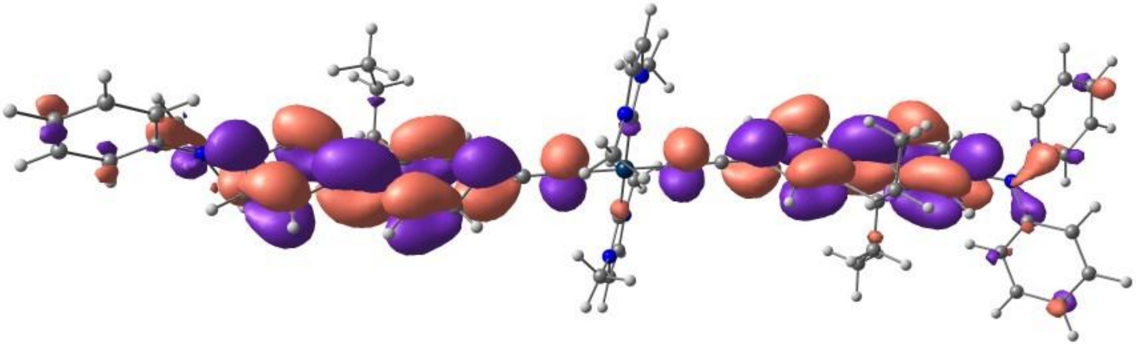

Figure 45. LUMO (orbital 281) of compound **2c**.

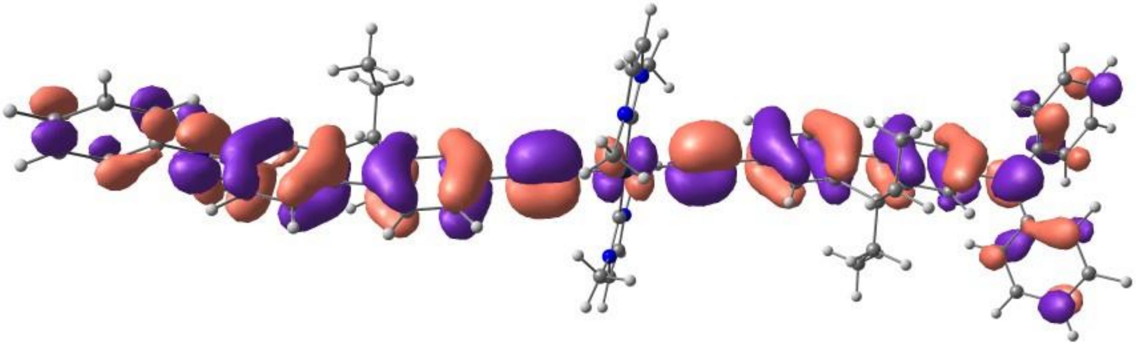

Figure 46. HOMO (orbital 280) of compound **2c**.

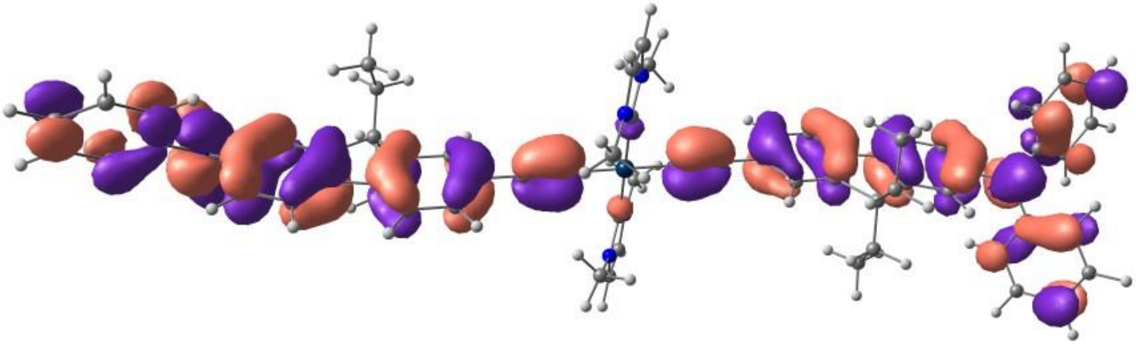

Figure 47. HOMO-1 (orbital 279) of compound **2c**.